


Giant Anisotropic Gilbert Damping in Single-Crystal Co-Fe-B(001) Films

Hongyue Xu^{1,†}, Haoran Chen^{1,†}, Fanlong Zeng¹, Jia Xu^{1,2}, Xi Shen¹, and Yizheng Wu^{1,3,*}

¹*Department of Physics and State Key Laboratory of Surface Physics, Fudan University, Shanghai 200433, China*

²*Department of Physics, School of Physics and Telecommunication Engineering, Shaanxi University of Technology, Hanzhong 723001, China*

³*Shanghai Research Center for Quantum Sciences, Shanghai 201315, China*

 (Received 13 October 2022; revised 22 December 2022; accepted 18 January 2023; published 10 February 2023)

We investigate the anisotropy of Gilbert damping in Co-Fe-B(001) films with body-centered-cubic crystalline structure using the ferromagnetic resonance method. The Co-Fe-B(001) films are epitaxied on MgO(001) by means of pulsed-laser deposition using a $\text{Co}_{0.4}\text{Fe}_{0.4}\text{B}_{0.2}$ target. The measured damping constant shows a clear four-fold symmetry with respect to the in-plane field orientation with a maximum-minimum ratio larger than 650%, and maximum damping exists for the field along Co-Fe-B(100). Such a large damping anisotropy can trigger the strong field-orientation dependence of microwave-excited magnetization precession. The anisotropic magnetoresistance (AMR) in Co-Fe-B(001) films shows little current-orientation dependence, indicating that AMR has weak correlation with the origin of damping anisotropy. Our experimental results provide an effective way to control intrinsic damping with magnetization orientation for designing and optimizing the performance of spintronics devices based on Co-Fe-B.

DOI: [10.1103/PhysRevApplied.19.024030](https://doi.org/10.1103/PhysRevApplied.19.024030)

I. INTRODUCTION

Gilbert damping plays a major role in emerging applications of spintronics, since it determines the energy relaxation rate of magnetization precession [1–4] and governs the critical current of magnetization switching [2,5–7], the velocity of domain-wall motion [1,8], and the spin-wave propagation [8,9]. The larger damping can trigger faster magnetization switching, and the lower damping enables more energy-efficient excitations and longer spin-wave propagation length. Therefore, it is crucial to explore the capability of controlling intrinsic damping for designing and optimizing the performance of spintronics devices.

Intrinsic Gilbert damping has been theoretically predicted to be associated with the band structure and can be changed with the magnetization orientation [10,11]. Most early experimental studies of intrinsic damping anisotropy were too weak for practical applications [12,13]. In epitaxial $\text{Co}_{0.5}\text{Fe}_{0.5}$ thin films, a giant Gilbert-damping anisotropy with a maximum-minimum ratio of 400% has been reported [14–16], which was attributed to the variation of spin-orbit coupling (SOC) depending on magnetization orientation. However, such giant damping anisotropy cannot be reproduced by the first-principles calculation, and only a 200% anisotropy ratio was achieved

due to the interfacial SOC [17]. Thus, in order to clarify the microscopic mechanism of anisotropic damping, it is highly desirable to explore Gilbert damping with strong anisotropy in different magnetic systems.

It is well known that the Co-Fe-B thin film has been widely applied in spintronics devices due to the large tunneling magnetoresistance (TMR) ratio in MgO-based magnetic tunnel junctions (MTJs) [18–20]. In most Co-Fe-B/MgO/Co-Fe-B based MTJ devices, the Co-Fe-B layers are usually highly textured with the body-centered-cubic (bcc) structure [19,20], and the bcc Co-Fe-B film can also be epitaxially grown on MgO(001) [21]. Thus, it should be highly interesting to explore whether a Co-Fe-B layer with bcc structure can exhibit similar strong anisotropic damping, which should influence the performance of spintronics devices based on Co-Fe-B layers. In this paper, we show that single-crystal Co-Fe-B film epitaxied on MgO(001) contains a strong anisotropy of Gilbert damping with a maximum-minimum ratio greater than 650%. The magnetization-orientation-dependent damping constant shows a clear four-fold symmetry with the maximum for the field along Co-Fe-B(100). Such damping anisotropy can trigger strong anisotropy of microwave-excited magnetization precession. Weak current-orientation effect of anisotropic magnetoresistance (AMR) was observed in the Co-Fe-B layer, which disproves the correlation between anisotropic damping and AMR, as discussed in the $\text{Co}_{0.5}\text{Fe}_{0.5}$ system [14]. Our

* wuyizheng@fudan.edu.cn

† These authors contributed equally.

studies not only provide an interesting material system with strong damping anisotropy for further exploring the intrinsic mechanism of anisotropic magnetic damping, but also could trigger subsequent studies on the effect of anisotropic damping in spintronics devices based on the Co-Fe-B layer.

II. EXPERIMENTS

Single-crystal Co-Fe-B films are prepared on MgO(001) substrates in an ultrahigh vacuum (UHV) chamber [22]. The MgO(001) substrate is first annealed at 600 °C for 30 min in the UHV system, and a 10-nm MgO seed layer is grown at 300 °C to improve the surface quality, which is confirmed by sharp reflection high-energy electron diffraction (RHEED) patterns, as shown in Fig. 1(a). The Co-Fe-B alloy films are epitaxially deposited on the MgO(001) substrates at 400 °C by pulsed-laser deposition (PLD) with a 248-nm KrF excimer laser from a $\text{Co}_{0.4}\text{Fe}_{0.4}\text{B}_{0.2}$ alloy target. Figure 1(b) shows the typical RHEED pattern from a 10 nm Co-Fe-B film with the electron beam directed along the MgO(100) direction. The clear elongated spots in the RHEED pattern demonstrate the epitaxial growth of the Co-Fe-B film. Because the MgO lattice constant is approximately $\sqrt{2}$ times larger than that of bcc Co-Fe-B, the Co-Fe-B film should have the epitaxial relationship of $\text{Co-Fe-B}\langle 110\rangle(001)//\text{MgO}\langle 100\rangle(001)$ [21]. Before being taken out from the UHV system, the samples are covered with a 6-nm-thick MgO capping layer to prevent oxidation. All film thicknesses are determined by the deposition rate (approximately 1.0–2.0 Å/min), which is measured using a calibrated quartz thickness monitor.

The crystal structure of the Co-Fe-B alloy film is also characterized by x-ray diffraction (XRD). Figure 1(c) shows a single peak at 64.4° in a wide angle range beside the peaks from the MgO(001) substrate. The determined lattice constant of Co-Fe-B from the XRD data is 2.89 Å, which is slightly larger than that of CoFe film grown on MgO(001) [14]. The magnetic properties of the Co-Fe-B film are firstly characterized by the longitudinal magneto-optic Kerr effect (MOKE) at room temperature. Figure 1(d) shows the hysteresis loops with the field H along $\text{Co-Fe-B}\langle 100\rangle$ and $\text{Co-Fe-B}\langle 110\rangle$. Both loops saturate for the field above 200 Oe, and the saturation field for $H//\text{Co-Fe-B}\langle 110\rangle$ is smaller.

The anisotropy of Gilbert damping in single-crystal Co-Fe-B alloy films was first investigated by the spin-torque ferromagnetic resonance (ST FMR) method at room temperature. We further grew a 3-nm Pt layer on top of the MgO(6 nm)/Co-Fe-B(10 nm)/MgO(001) sample, then pattern it into the microwave antenna device through the ordinary photolithography and Ar^+ bombardment process. The size of the antenna devices is $100 \times 10 \mu\text{m}^2$, with the orientation 60° away from $\text{Co-Fe-B}\langle 110\rangle$

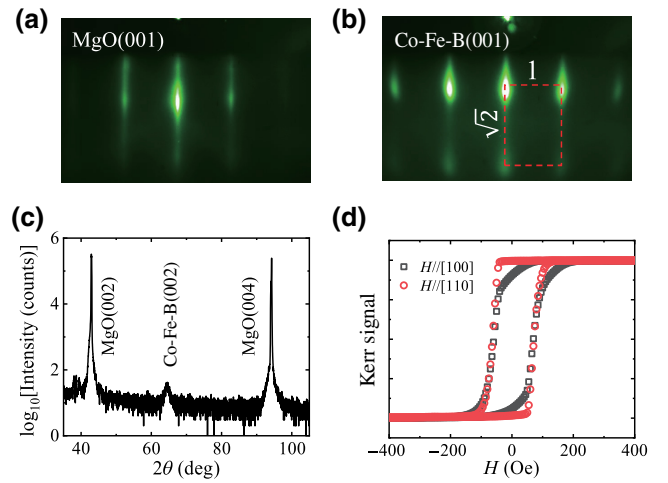


FIG. 1. (a),(b) Typical RHEED patterns from (a) MgO(001) substrate and (b) a 10-nm-thick Co-Fe-B(001) film with the electron incident along MgO(100). (c) The x-ray diffraction spectra of a 10-nm-thick Co-Fe-B(001) film grown on MgO(001). (d) Typical hysteresis loops with H along $\text{Co-Fe-B}\langle 100\rangle$ and $\text{Co-Fe-B}\langle 110\rangle$, respectively.

direction. Contacts are made of a 10-nm-thick Cr layer covered by a 150-nm-thick Au layer. The microwave current through the Pt layer can induce an in-plane oscillating transverse field in the Co-Fe-B layer, and then excites the resonance of Co-Fe-B magnetization. A dc voltage V_{dc} can be detected by the spin-rectification (SR) signal due to the magnetoresistance variation caused by the magnetization precession [23]. The 6-nm MgO layer is thick enough to isolate the transmission of the spin current between Co-Fe-B and Pt, thus, the spin-torque effect from the Pt layer and the spin pumping effect should be suppressed in the FMR measurements [24,25]. The ST FMR measurement is performed in a vector electromagnet system with a maximum field of 3 kOe.

Anisotropic damping of the Co-Fe-B layer is also determined through the microwave adsorption measurement with a broadband coplanar waveguide (CPW) in a vector superconducting magnet. The sample is positioned on the signal line of the waveguide, and the transmission parameter S_{21} is measured using the vector network analyzer with the field sweeping along different in-plane directions.

III. RESULTS AND DISCUSSION

Figure 2(a) shows the typical ST FMR voltage spectra measured at $f = 16$ GHz with H along different directions. The ST FMR spectra are dominated with the antisymmetric lineshape due to the SR signal driven by the microwave field, which also proves the negligible spin-orbit torque effect in our ST FMR measurement [23]. The resonance field H_r shows little change for the field varying from $\langle 110\rangle$ ($\phi_H = 0^\circ$) to $\langle 100\rangle$ ($\phi_H = 45^\circ$), indicating a weak

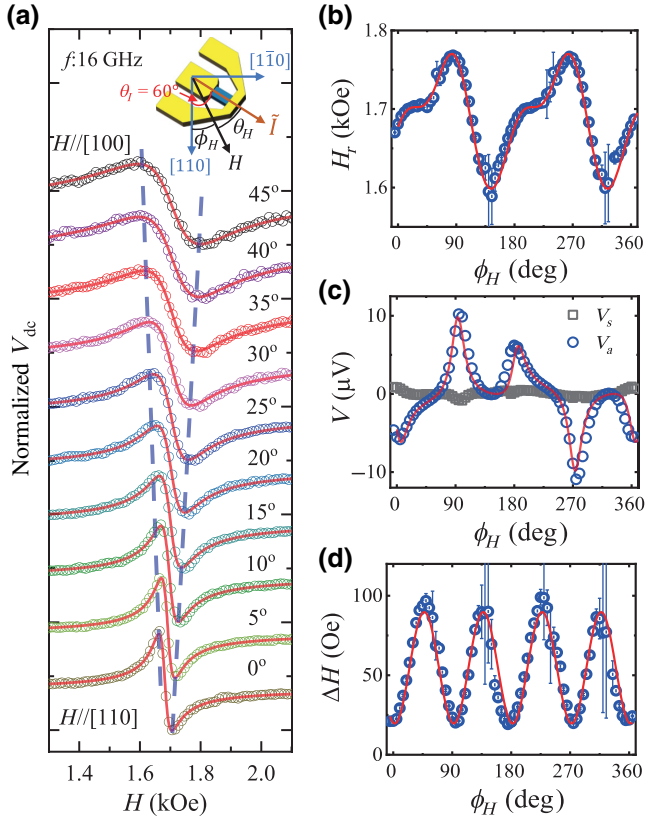


FIG. 2. (a) Typical FMR spectra detected with different ϕ_H from a device with a current orientation angle of $\theta_I = 60^\circ$. The microwave frequency is 16 GHz. The inset shows the geometry of the measured ST FMR device. (b)–(d) The fitted resonance field H_r , the symmetrical and asymmetrical voltages V_s and V_a , and the linewidth ΔH as a function of ϕ_H . The solid lines are the fitting curves as described in the main text.

magnetic anisotropy in this sample. As emphasized by the purple dashed lines, the linewidth ΔH of the resonant peak shows a strong increase for ϕ_H increasing from 0° to 45° .

The voltage spectra in Fig. 2(a) can be quantitatively fitted by a combination of symmetric and antisymmetric Lorentzian functions [23]

$$V_{dc} = V_s \frac{\Delta H^2}{(H - H_r)^2 + \Delta H^2} + V_a \frac{\Delta H(H - H_r)}{(H - H_r)^2 + \Delta H^2}, \quad (1)$$

where V_s and V_a are the magnitude of symmetric and anti-symmetric voltages, respectively. The parameters H_r , V_s , V_a , and ΔH as a function of ϕ_H can be determined through the fitting, as shown in Figs. 2(b)–2(d). Figure 2(b) shows the ϕ_H dependence of H_r with $f = 16$ GHz. The variation of H_r is less than 170 Oe, much smaller than the H_r value of approximately 1.7 kOe, indicating very small magnetic anisotropy in the Co-Fe-B film. The $H_r(\phi_H)$ curve also indicates the presence of twofold and fourfold magnetic anisotropies. The $H_r(\phi_H)$ curve in Fig. 2(b) can be well

fitted by the modified Kittel formula [26,27]

$$\left(\frac{\omega}{\gamma}\right)^2 = \mu_0^2 H_r' H_r'', \quad (2)$$

with $H' = H \cos(\phi_M - \phi_H) + M_s + H_4(3 - \cos 4\phi_M)/4 - H_u \cos^2 \phi_M$ and $H'' = H \cos(\phi_M - \phi_H) - H_4 \cos 4\phi_M + H_u \cos 2\phi_M$. H_r' and H_r'' represent the magnitudes of H' and H'' , respectively, while H is equal to H_r . Here, γ is the gyromagnetic ratio, ϕ_M is the angle between the magnetization and Co-Fe-B[110], M_s is the saturation magnetization, H_4 is the fourfold anisotropy field with easy axis along $\langle 110 \rangle$, and H_u is the uniaxial anisotropy field with easy axis along $[010]$. By fitting the $H_r(\phi_H)$ data with the red line, we determine the saturation magnetization $M_s = 14.7$ kOe, the Landé g factor $g = 2.17$, the fourfold anisotropy field $H_4 = 35$ Oe with easy axis along $\langle 110 \rangle$, and the uniaxial anisotropy field $H_u = 70$ Oe with easy axis along $\langle 100 \rangle$. Note that M_s and H_4 for 10 nm CoFe(001) film grown on MgO(001) are 24.5 kOe and 270 Oe, respectively [15]. Although the stoichiometry in the Co_{0.4}Fe_{0.4}B_{0.20} target, the determined magnetization and weak magnetic anisotropy agree well with the properties of Co-Fe-B films reported in the literature [28–30].

Figure 2(c) shows the fitted ϕ_H dependence of V_s and V_a , and V_s is one order larger than V_a . In Fig. 2(d), we plot the ϕ_H dependence of the linewidth ΔH , which clearly exhibits a fourfold symmetry with a maximum for $H \parallel \langle 100 \rangle$ and a minimum for $H \parallel \langle 110 \rangle$. The ϕ_H -dependent ΔH has a different symmetry from that of H_r , so the damping anisotropy is not simply correlated with the magnetic anisotropy. Note that the SR signal should be close to zero for the field along or perpendicular to the sample strips in ST FMR devices [23], thus the signal V_a in Fig. 2(c) for $\phi_H \sim 60^\circ, 150^\circ, 240^\circ, 330^\circ$ is close to 0, and around those field angles, the fitted H_r in Fig. 2(b) and ΔH in Fig. 2(d) exhibit larger error bars.

Next, we show that the damping constant α in the Co-Fe-B(001) film has strong anisotropy. In general, α can be extracted by fitting the frequency-dependent ΔH with the formula $\Delta H = \Delta H_{inh} + 2\pi f \alpha / \gamma$. ΔH_{inh} is the inhomogeneous broadening due to the disorders in the film. Figure 3(a) shows that the fitted ΔH has a linear dependence on f between 7 and 20 GHz with H along different directions. All the resonant fields are larger than 400 Oe for $f > 7$ GHz, thus due to the weak magnetic anisotropy in Co-Fe-B film, the magnetization for all the measurements in Fig. 2(a) is aligned well along the field direction, i.e., $\phi_H \sim \phi_M$. Figure 2(a) also shows that the slope of $\Delta H(f)$ has a strong change with ϕ_H , but the similar intercept ΔH_{inh} around approximately 22 Oe can be obtained for all field orientations. The fitted damping constant is $\alpha_{[110]} = 0.0040 \pm 0.0001$ for $H \parallel [110]$ ($\phi_H = 0^\circ$) and $\alpha_{[100]} = 0.0322 \pm 0.0004$ for $H \parallel [100]$ ($\phi_H = 45^\circ$),

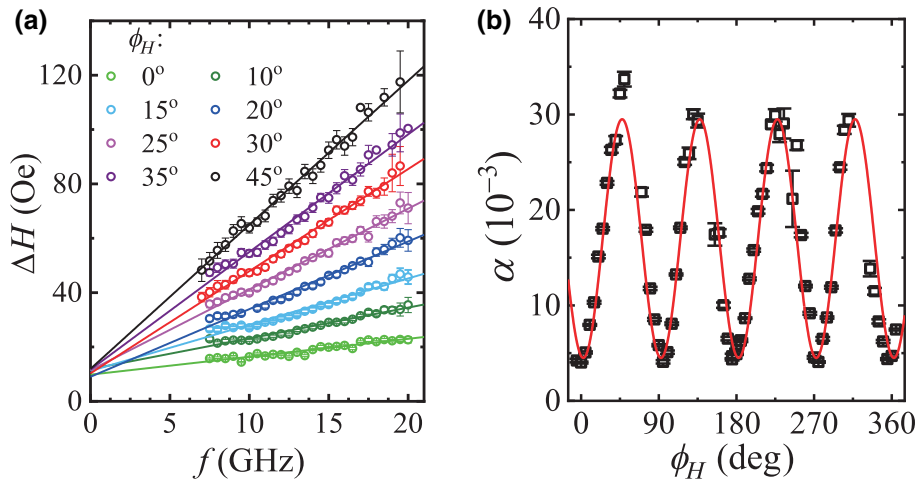


FIG. 3. (a) FMR linewidth as a function of frequency for the selected ϕ_H s. (b) The measured damping constant as a function of ϕ_H . The solid lines are fitting curves as described in the main text.

thus the damping constant in the Co-Fe-B(001) film has an anisotropy ratio of 805%, which is much larger than that of 440% in $\text{Co}_{0.5}\text{Fe}_{0.5}$ (001) films [14]. We perform the SR measurements for all the field orientations, and the obtained ϕ_H -dependent α in Fig. 3(b) has a clear fourfold symmetry, which can be well fitted by the equation $\alpha(\phi_H) = \alpha_0 - \Delta\alpha \cos(4\phi_H)$. The fitting results in an anisotropy ratio $(\alpha_0 + \Delta\alpha)/\alpha_0 - \Delta\alpha$ of 650%. Note that no damping data can be obtained for $\phi \sim 60^\circ, 150^\circ, 240^\circ, 330^\circ$, since the SR signal is close to zero around those field orientations in our device.

The fourfold symmetry of α in Fig. 3(b) indicates the anisotropic intrinsic Gilbert damping in Co-Fe-B(001) associates with its crystal structure. Our measurements can further rule out extrinsic contributions to the anisotropic damping, such as a mosaic effect due to lattice disorder in the epitaxial film [31–33], magnetic drag effect [34–36], and two-magnon scattering (TMS) effect [33,36–42]. The mosaic effect on damping is induced by the lattice disorder due to the epitaxial strain in the film [31–33]. The epitaxial growth of Co-Fe-B film on a MgO(001) surface may induce a fourfold lattice disorder, which could further influence the effective damping in the film. However, the lattice disorder also strongly influences ΔH_{inh} as well. Figure 3(a) indicates that ΔH_{inh} is almost independent of the field orientation, which can rule out the correlation between the observed damping anisotropy and the possible lattice disorder in Co-Fe-B(001) film.

In the system with strong in-plane anisotropy, the magnetic drag effect can result in resonant linewidth broadening and nonlinear dependence of linewidth on frequency stemming from field-magnetization misalignment [12,15,34], thus it may influence the determination of the intrinsic damping constant using the FMR technique [33,34,36,37]. However, the magnetic drag effect strongly depends on magnetic anisotropy, and a fourfold anisotropy

can induce the anisotropic linewidth broadening with an eightfold symmetry [34,40]. In our Co-Fe-B(001) system, the damping anisotropy and the magnetic anisotropy have no correlation, since our sample contains both twofold and fourfold magnetic anisotropies, but shows only a clear fourfold damping symmetry. Moreover, the magnetic drag effect can be well suppressed by a strong magnetic field [8,10]. In the Co-Fe-B(001) film, the in-plane fourfold anisotropy field is only approximately 35 Oe, so it is hard to induce a significant magnetic drag effect for the field above 400 Oe in our experiments.

The TMS contribution commonly exists in thin films with the magnetization aligned in the film plane [33, 36,38]. Due to dipolar coupling, the short wavelength spin waves can degenerate with the FMR mode, thus the defects can scatter the FMR mode into such short wavelength spin waves, which makes ΔH nonlinearly dependent on f . In thin films with weak in-plane anisotropy, the spin-wave dispersion should have weak dependence on the magnetization orientation, thus the related TMS contribution should not strongly depend on the magnetization orientation. The TMS contribution ΔH_{TMS} can be expressed as [41,42]

$$\Delta H_{\text{TMS}} = \Gamma \sin^{-1} \frac{\sqrt{\omega^2 + (\omega_0/2)^2} - \omega_0/2}{\sqrt{\omega^2 + (\omega_0/2)^2} + \omega_0/2}, \quad (3)$$

where Γ is the TMS strength, $\omega_0 = \gamma\mu_0 M_{\text{eff}}$, and M_{eff} is the effective magnetization. ΔH_{TMS} has a steep nonlinear slope at low frequencies, and saturates at high frequencies. Thus, the TMS contribution should be suppressed at strong field with high resonant frequency [33,38].

We perform wide-band microwave-absorption measurements on a MgO(6 nm)/Co-Fe-B(10 nm)/MgO(001) film

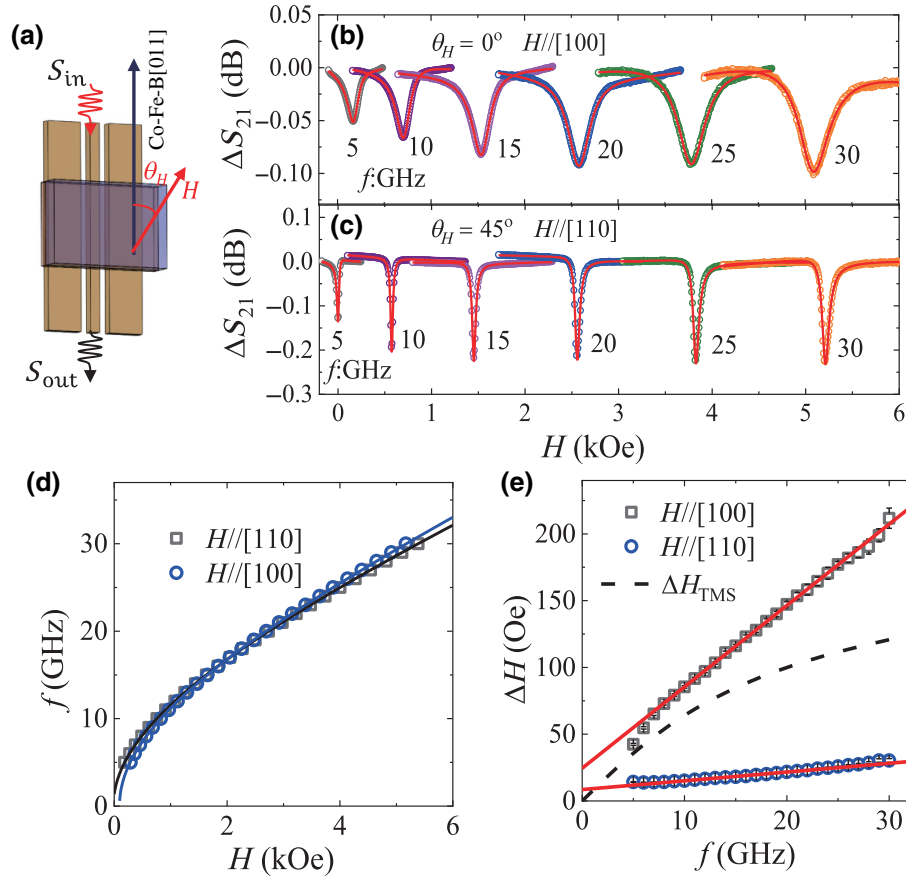


FIG. 4. (a) Sample geometry for the microwave adsorption FMR measurement. (b),(c) Typical FMR spectra detected with different f for the field along (b) Co-Fe-B[100] and (c) Co-Fe-B[110], respectively. The solid lines are the fitting curves with Eq. (1). (d) FMR dispersion for $H//\text{Co-Fe-B}[100]$ and $H//\text{Co-Fe-B}[110]$, respectively. The solid lines are the fitting curves with Eq. (2). (e) The f -dependent ΔH for $H//\text{Co-Fe-B}[100]$ and $H//\text{Co-Fe-B}[110]$, respectively. The black dashed line is the TMS contribution to the FMR linewidth calculated with Eq. (3).

in a vector superconducting magnet as shown in Fig. 4(a). Figures 4(b) and 4(c) show the typical FMR absorption spectra at different frequencies for $H//[100]$ and $H//[110]$, respectively. The FMR absorption spectra can be well measured for frequencies up to 30 GHz. The linewidth for $H//[100]$ is clearly much larger than that for $H//[110]$. Through the fitting with Eq. (1), we can obtain the f -dependent H_r and ΔH . In Fig. 4(d), the $H_r - f$ relations for $H//[100]$ and $H//[110]$ have very little difference, which further confirms the weak in-plane magnetic anisotropy in the Co-Fe-B film. The linewidth ΔH shows good linear dependence for f up to 30 GHz for both field orientations, proving that the anisotropic damping is unlikely related to TMS. Through the linear $\Delta H - f$ relations in Fig. 4(e), we can obtain the damping constants $\alpha_{[100]} = 0.0368 \pm 0.0001$ and $\alpha_{[110]} = 0.0039 \pm 0.0002$ with an the anisotropic ratio of $(\alpha_{[100]}/\alpha_{[110]}) \sim 944\%$, larger than the results obtained in ST FMR measurements in Fig. 3(b). We also calculate the f -dependent ΔH_{TMS} with $\Gamma = 150$ Oe and $\mu_0 M_{\text{eff}} =$

14.7 kOe, as shown by the dashed line in Fig. 4(e). The calculated ΔH_{TMS} shows strong nonlinearity at approximately 15 GHz, and the experimental data shows very good linear dependence for f between 7 and 30 GHz, so our experimental data demonstrates that TMS has little contribution to the measured giant anisotropy of the intrinsic damping in the Co-Fe-B(001) system.

We also perform the temperature-dependent wide-band microwave-adsorption measurement. The measured $\alpha_{[100]}$ is almost independent of temperature. The temperature-dependent $\alpha_{[110]}$ shows a nonmonotonic behavior with the maximum at approximately 50 K, and the maximum variation is less than 30%. So, the damping mechanism of the Co-Fe-B layer is different with that in the CoFe(001) system, which shows the conductivitylike damping behavior [14]. It should be noted that the crystalline quality of Co-Fe-B(001) film is much poorer in comparison with CoFe(001) film, thus the impurity in Co-Fe-B film may play a significant role on damping, which is expected to be less temperature dependent.

So far, the physical origin of large Gilbert-damping anisotropy is still not well understood, although the intrinsic damping is believed to be determined by the inter-band or intraband electron scatterings [10,43,44]. In Ref. [15], the large damping anisotropy in CoFe(001) film is attributed to the anisotropy of spin-orbit coupling (SOC) related to crystal directions, which correlates with the anisotropies of Gilbert damping and anisotropic magnetoresistance (AMR). However, we find that the observed giant damping anisotropy in the crystal Co-Fe-B film has a weak correlation with the current-orientation dependent AMR. We make several Hall bars with the current flowing along different crystal angles. Figure 5(a) shows the angular-dependent resistances for the current I along $\langle 100 \rangle$ and $\langle 110 \rangle$. Both AMR curves show twofold angular dependence with the maximum for the field along the current direction, consistent with the ordinary AMR effect in most magnetic metal systems. The AMR effect for $I//\langle 100 \rangle$ is slightly larger than that for $I//\langle 110 \rangle$. If defining the AMR ratio with $(R_{\max} - R_{\min})/R_{\min}$, the measured AMR ratio in Fig. 5(b) shows a clear fourfold symmetry with the current orientation, but the AMR ratios for $I//\langle 100 \rangle$ and $I//\langle 110 \rangle$ only show an 80% difference, which is one order smaller than the AMR anisotropy in CoFe(001) films [22]. Note that the ultrafast demagnetization in CoFe(001) film excited by the femtosecond laser is found to be isotropic [16]. Our studies suggest that intrinsic damping, AMR, and ultrafast demagnetization may originate from different mechanisms, although all these three important magnetic properties should be correlated with the SOC in magnetic systems.

Co-Fe-B film has been widely applied in spintronics devices like MRAM [18,45,46], thus the damping anisotropy should influence the performance of these spintronics devices based on the magnetization reversal in Co-Fe-B film. In Fig. 2(c), the angular-dependent SR signal clearly deviates from the standard $\sin 2\theta_M \cos \theta_M$ function in most ST FMR studies [23,47–49], which can be attributed to the effect of damping anisotropy in Co-Fe-B film. Here, θ_M is defined as the angle between the magnetization and the microwave current. The θ_M -dependent SR signal V_a can be expressed as $V_a \propto (\gamma H' / (\alpha \omega (H' + H''))) \sin 2\theta_M \cos \theta_M$ with H' and H'' defined in Eq. (2) [23]. Due to the small in-plane magnetic anisotropy, H' and H'' have very weak dependence on θ_M . Figure 3 already shows that α strongly depends on ϕ_H with a function of $\cos(4\phi_H)$. If considering the offset angle of 60° between ϕ_H and θ_M , the SR signal V_a can be expressed as $V_a \propto (\sin 2(60 - \phi_H) \cos(60 - \phi_H)) / (\alpha_0 - \Delta \alpha \cos(4\phi_H))$, which can well fit the experimental curve, as shown by the red line in Fig. 2(c). Moreover, the microwave-adsorption data in Fig. 4 also demonstrates that the resonant adsorption signal for $H//\langle 110 \rangle$ with small α is much larger than that for $H//\langle 100 \rangle$ with large α . Therefore, our results well prove

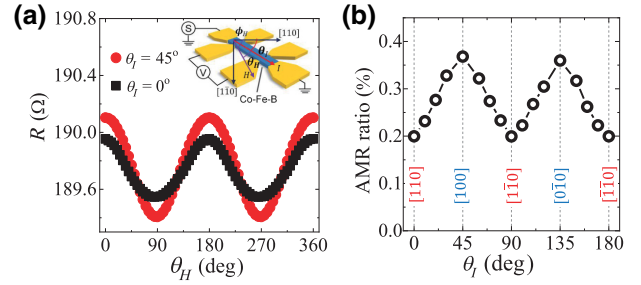


FIG. 5. (a) The θ_H -dependent magnetoresistance for currents applied along Co-Fe-B[110] ($\theta_I = 0^\circ$) and Co-Fe-B[100] ($\theta_I = 45^\circ$) in a Co-Fe-B(10 nm)/MgO(001) sample. The inset shows the schematic of the device with the definition of θ_H and θ_I . (d) The measured θ_I dependence of AMR ratios.

that the microwave-excited magnetization dynamical properties in single-crystal Co-Fe-B film should have strong anisotropic dependence on the magnetization orientation. The Co-Fe-B layers in MRAM devices are expected to have a bcc-textured structure [29,30], so the magnetization dynamics in MRAM devices should also strongly depend on the magnetization orientation, thus our discovery on giant damping anisotropy in Co-Fe-B films provides a tuning parameter to manipulate the performance of the devices. The effect of anisotropic damping in MRAM devices based on Co-Fe-B layers still requires future investigation.

IV. SUMMARY

Our experimental results demonstrate the existence of giant anisotropic Gilbert damping in single-crystal Co-Fe-B(001) films. The measured Gilbert-damping constant shows a maximum value for $H//\langle 100 \rangle$ and the minimum value for $H//\langle 110 \rangle$ with a clear in-plane fourfold symmetry. The maximum damping anisotropy ratio determined by the microwave adsorption FMR is 944%. Due to the weak in-plane magnetic anisotropy, the extrinsic contributions to the measured anisotropic damping by the magnetic drag effect and the two-magnon scattering effect have been ruled out. Weak current-orientation-dependent AMR is observed in Co-Fe-B film, indicating that AMR has a weak correlation with the strong damping anisotropy. Our results call for further theoretical studies to reveal the underlying mechanism of the giant anisotropy damping in Co-Fe-B film. Our experiments also prove that the damping anisotropy indeed makes microwave-excited magnetization dynamics strongly dependent on the field orientation, which can pave an effective way to design and optimize spintronics devices based on the Co-Fe-B layer.

ACKNOWLEDGMENTS

This work is supported by the National Key Research Program of China (Grant No. 2022YFA1403300), the

National Natural Science Foundation of China (Grants No. 11974079, No. 11734006, No. 12274083, and No. 12221004), the Shanghai Municipal Science and Technology Major Project (Grant No. 2019SHZDZX01) and the Shanghai Municipal Science and Technology Basic Research Project (No. 22JC1400200). Jia Xu acknowledges support by National Natural Science Foundation of China (Grant No. 12204295), Natural Science Foundation of Shaanxi Provincial Department of Education (Grant No. 22JK0310), Natural Science Basic Research Program of Shaanxi (Grant No. 2022JQ-017), Shaanxi University of Technology (SLGRCQD2125).

-
- [1] A. Bland and B. Heinrich, *Ultrathin Magnetic Structures* (Springer, Berlin; New York, 1994), Vol. 4.
- [2] A. Hirohata, K. Yamadab, Y. Nakatanic, I.-L. Prejbeanud, B. Diényd, P. Pirroo, and B. Hillebrands, Review on spintronics: Principles and device applications, *J. Magn. Magn. Mater.* **509**, 166711 (2020).
- [3] A. Barman, G. Gubbiotti, S. Ladak, A. O. Adeyeye, M. Krawczyk, J. Gräfe, C. Adelmann, S. Cotofana, A. Naeemi, V. I. Vasyuchka, *et al.*, The 2021 Magnonics Roadmap, *J. Phys.: Condens. Matter* **33**, 413001 (2021).
- [4] M. Fähnle and C. Illg, Electron theory of fast and ultrafast dissipative magnetization dynamics, *J. Phys.: Condens. Matter* **23**, 493201 (2011).
- [5] D. C. Ralph and M. D. Stiles, Spin transfer torques, *J. Magn. Magn. Mater.* **320**, 1190 (2008).
- [6] A. V. Khvalkovskiy, D. Apalkov, S. Watts, R. Chepulskii, R. S. Beach, A. Ong, X. Tang, A. Driskill-Smith, W. H. Butler, P. B. Visscher, *et al.*, Basic principles of STT-MRAM cell operation in memory arrays, *J. Phys. D: Appl. Phys.* **46**, 074001 (2013).
- [7] S. Bhatti, R. Sbiaa, A. Hirohata, H. Ohno, S. Fukami, and S. N. Piramanayagam, Spintronics based random access memory: A review, *Mater. Today* **20**, 530 (2017).
- [8] T. Weindler, H. G. Bauer, R. Islinger, B. Boehm, J.-Y. Chauleau, and C. H. Back, Magnetic Damping: Domain Wall Dynamics versus Local Ferromagnetic Resonance, *Phys. Rev. Lett.* **113**, 237204 (2014).
- [9] A. V. Chumak, V. I. Vasyuchka, A. A. Serga, and B. Hillebrands, Magnon spintronics, *Nat. Phys.* **11**, 453 (2015).
- [10] A. Brataas, Y. Tserkovnyak, and G. E. W. Bauer, Scattering Theory of Gilbert Damping, *Phys. Rev. Lett.* **101**, 037207 (2008).
- [11] K. Gilmore, M. D. Stiles, J. Seib, D. Steiauf, and M. Fähnle, Anisotropic damping of the magnetization dynamics in Ni, Co, and Fe, *Phys. Rev. B* **81**, 174414 (2010).
- [12] L. Chen, S. Mankovsky, S. Wimmer, M. A. W. Schoen, H. S. Körner, M. Kronseder, D. Schuh, D. Bougeard, H. Ebert, D. Weiss, *et al.*, Emergence of anisotropic Gilbert damping in ultrathin Fe layers on GaAs(001), *Nat. Phys.* **14**, 490 (2018).
- [13] W. Zhang, Y. Li, N. Li, Y. Li, Z. Z. Gong, X. Yang, Z. K. Xie, R. Sun, X. Q. Zhang, W. He, *et al.*, Strongly enhanced gilbert damping anisotropy at low temperature in high quality single-crystalline Fe/MgO(001) thin film, *J. Magn. Magn. Mater.* **496**, 165950 (2020).
- [14] Y. Li, F. L. Zeng, S. S.-L. Zhang, H. Shin, H. Saglam, V. Karakas, O. Ozatay, J. E. Pearson, O. G. Heinonen, Y. Z. Wu, *et al.*, Giant Anisotropy of Gilbert Damping in Epitaxial CoFe Films, *Phys. Rev. Lett.* **122**, 117203 (2019).
- [15] F. Zeng, X. Shen, Y. Li, Z. Yuan, W. Zhang, and Y. Wu, Role of crystalline and damping anisotropy to the angular dependences of spin rectification effect in single crystal CoFe, *New J. Phys.* **22**, 093047 (2020).
- [16] H. Xia, Z. R. Zhao, F. L. Zeng, H. C. Zhao, J. Y. Shi, Z. Zheng, X. Shen, J. He, G. Ni, Y. Z. Wu, *et al.*, Giant anisotropic Gilbert damping versus isotropic ultrafast demagnetization in monocrystalline Co₅₀Fe₅₀ films, *Phys. Rev. B* **104**, 024404 (2021).
- [17] I. P. Miranda, A. B. Klautau, A. Bergman, D. Thonig, H. M. Petrilli, and O. Eriksson, Mechanisms behind large Gilbert damping anisotropies, *Phys. Rev. B* **103**, L220405 (2021).
- [18] S. Ikeda, J. Hayakawa, Y. Ashizawa, Y. M. Lee, K. Miura, H. Hasegawa, M. Tsunoda, F. Matsukura, and H. Ohno, Tunnel magnetoresistance of 604% at 300 K by suppression of Ta diffusion in CoFeB/MgO/CoFeB pseudo-spin-valves annealed at high temperature, *Appl. Phys. Lett.* **93**, 082508 (2008).
- [19] S. Ikeda, J. Hayakawa, Y. M. Lee, F. Matsukura, Y. Ohno, T. Hanyu, and H. Ohno, Magnetic tunnel junctions for spintronic memories and beyond, *IEEE Trans. Electron Devices* **54**, 991 (2007).
- [20] Y. M. Lee, J. Hayakawa, S. Ikeda, F. Matsukura, and H. Ohno, Effect of electrode composition on the tunnel magnetoresistance of pseudo-spin-valve magnetic tunnel junction with a MgO tunnel barrier, *Appl. Phys. Lett.* **90**, 212507 (2007).
- [21] A. K. Kaveev, V. E. Bursian, B. B. Krichevtsov, K. V. Mashkov, S. M. Sutturin, M. P. Volkov, M. Tabuchi, and N. S. Sokolov, Laser MBE-grown CoFeB epitaxial layers on MgO: Surface morphology, crystal structure, and magnetic properties, *Phys. Rev. Mater.* **2**, 014411 (2018).
- [22] F. L. Zeng, Z. Y. Ren, Y. Li, J. Y. Zeng, M. W. Jia, J. Miao, A. Hoffmann, W. Zhang, Y. Z. Wu, and Z. Yuan, Intrinsic Mechanism for Anisotropic Magnetoresistance and Experimental Confirmation in Co_xFe_{1-x} Single-Crystal Films, *Phys. Rev. Lett.* **125**, 097201 (2020).
- [23] M. Harder, Y. Gui, and C.-M. Hu, Electrical detection of magnetization dynamics via spin rectification effects, *Phys. Rep.* **661**, 1 (2016).
- [24] O. Mosendz, J. E. Pearson, F. Y. Fradin, G. E. W. Bauer, S. D. Bader, and A. Hoffmann, Quantifying Spin Hall Angles from Spin Pumping: Experiments and Theory, *Phys. Rev. Lett.* **104**, 046601 (2010).
- [25] L. Mihalceanu, S. Keller, J. Greser, D. Karfaridis, K. Symeonidis, G. Vourlias, T. Kehagias, A. Conca, B. Hillebrands, and E. T. Papaioannou, Spin-pumping through a varying-thickness MgO interlayer in Fe/Pt system, *Appl. Phys. Lett.* **110**, 252406 (2017).
- [26] C. Kittel, On the theory of ferromagnetic resonance absorption, *Phys. Rev.* **73**, 155 (1948).
- [27] O. Kohmoto, Effective demagnetizing factors of second-order magnetocrystalline anisotropies in ferromagnetic resonance Kittel formula, *Jpn. J. Appl. Phys.* **43**, 6 (2004).

- [28] C. Bilzer, T. Devolder, J.-V. Kim, G. Counil, C. Chappert, S. Cardoso, and P. P. Freitas, Study of the dynamic magnetic properties of soft CoFeB films, *J. Appl. Phys.* **100**, 053903 (2006).
- [29] T. Yamamoto, T. Ichinose, J. Uzuhashi, T. Nozaki, T. Ohkubo, K. Yakushiji, H. Kubota, A. Fukushima, K. Hono, and S. Yuasa, Perpendicular magnetic anisotropy and its voltage control in MgO/CoFeB/Mo/CoFeB/MgO junctions, *J. Phys. D: Appl. Phys.* **55**, 275003 (2022).
- [30] X. Liu, W. Zhang, M. J. Carter, and G. Xiao, Ferromagnetic resonance and damping properties of CoFeB thin films as free layers in MgO-based magnetic tunnel junctions, *J. Appl. Phys.* **110**, 033910 (2011).
- [31] R. D. McMichael, D. J. Twisselmann, and A. Kunz, Localized Ferromagnetic Resonance in Inhomogeneous Thin Films, *Phys. Rev. Lett.* **90**, 227601 (2003).
- [32] M. Belmeguenai, H. Tuzcuoglu, M. S. Gabor, T. Petrisor, C. Tiusan, D. Berling, F. Zighem, T. Chauveau, S. M. Cherif, and P. Moch, Co₂FeAl thin films grown on MgO substrates: Correlation between static, dynamic, and structural properties, *Phys. Rev. B* **87**, 184431 (2013).
- [33] Kh. Zakeri, J. Lindner, I. Barsukov, R. Meckenstock, M. Farle, U. von Hörsten, H. Wende, W. Keune, J. Rucker, S. S. Kalarickal, *et al.*, Spin dynamics in ferromagnets: Gilbert damping and two-magnon scattering, *Phys. Rev. B* **76**, 104416 (2007).
- [34] Y. Li, Y. Li, R. Sun, J. N. Liu, N. Li, X. Yang, Z. Z. Gong, Z. K. Xie, W. He, X. Q. Zhang, *et al.*, Drag effect induced large anisotropic damping behavior in magnetic thin films with strong magnetic anisotropy, *J. Phys.: Condens. Matter* **33**, 175801 (2021).
- [35] Yu. V. Goryunov, N. N. Garif'yanov, G. G. Khaliullin, I. A. Garifullin, L. R. Tagirov, F. Schreiber, Th. Mühge, and H. Zabel, Magnetic anisotropies of sputtered Fe films on MgO substrates, *Phys. Rev. B* **52**, 13450 (1995).
- [36] K. Lenz, H. Wende, W. Kuch, K. Baberschke, K. Nagy, and A. Jánossy, Two-magnon scattering and viscous Gilbert damping in ultrathin ferromagnets, *Phys. Rev. B* **73**, 144424 (2006).
- [37] R. Arias and D. L. Mills, Extrinsic contributions to the ferromagnetic resonance response of ultrathin films, *Phys. Rev. B* **60**, 7395 (1999).
- [38] G. Woltersdorf and B. Heinrich, Two-magnon scattering in a self-assembled nanoscale network of misfit dislocations, *Phys. Rev. B* **69**, 184417 (2004).
- [39] I. Barsukov, P. Landeros, R. Meckenstock, J. Lindner, D. Spoddig, Z.-A. Li, B. Krumme, H. Wende, D. L. Mills, and M. Farle, Tuning magnetic relaxation by oblique deposition, *Phys. Rev. B* **85**, 014420 (2012).
- [40] A. Conca, Separation of the two-magnon scattering contribution to damping for the determination of the spin mixing conductance, *Phys. Rev. B* **98**, 214439 (2018).
- [41] J. Lindner, I. Barsukov, C. Raeder, C. Hassel, O. Posth, R. Meckenstock, P. Landeros, and D. L. Mills, Two-magnon damping in thin films in case of canted magnetization: Theory versus experiment, *Phys. Rev. B* **80**, 224421 (2009).
- [42] J. Lindner, K. Lenz, E. Kosubek, K. Baberschke, D. Spoddig, R. Meckenstock, J. Pelzl, Z. Frait, and D. L. Mills, Non-Gilbert-type damping of the magnetic relaxation in ultrathin ferromagnets: Importance of magnon-magnon scattering, *Phys. Rev. B* **68**, 060102 (2003).
- [43] V. Kamberský, On the Landau–Lifshitz relaxation in ferromagnetic metals, *Can. J. Phys.* **48**, 2906 (1970).
- [44] V. Kamberský, On ferromagnetic resonance damping in metals, *Can. J. Phys.* **26**, 1366 (1976).
- [45] N. D. Rizzo, D. Houssameddine, J. Janesky, R. Whig, F. B. Mancoff, M. L. Schneider, M. DeHerrera, J. J. Sun, K. Nagel, S. Deshpande, *et al.*, A fully functional 64 Mb DDR3 ST-MRAM built on 90 nm CMOS technology, *IEEE Trans. Magn.* **49**, 4441 (2013).
- [46] J. Hayakawa, S. Ikeda, Y. M. Lee, F. Matsukura, and H. Ohno, Effect of high annealing temperature on giant tunnel magnetoresistance ratio of CoFeB/MgO/CoFeB magnetic tunnel junctions, *Appl. Phys. Lett.* **89**, 232510 (2006).
- [47] N. Mecking, Y. S. Gui, and C.-M. Hu, Microwave photovoltage and photoresistance effects in ferromagnetic microstrips, *Phys. Rev. B* **76**, 224430 (2007).
- [48] A. Yamaguchi, H. Miyajima, T. Ono, Y. Suzuki, S. Yuasa, A. Tulapurkar, and Y. Nakatani, Rectification of radio frequency current in ferromagnetic nanowire, *Appl. Phys. Lett.* **90**, 182507 (2007).
- [49] L. H. Bai, Y. S. Gui, A. Wirthmann, E. Recksiedler, N. Mecking, C.-M. Hu, Z. H. Chen, and S. C. Shen, The rf magnetic-field vector detector based on the spin rectification effect, *Appl. Phys. Lett.* **92**, 032504 (2008).